

Temperature dependent photoluminescence of Dy³⁺ doped LiCaBO₃ phosphor

Abhay Roshan Beck¹ · Sourav Das¹ · Jairam Manam¹

Received: 10 June 2017 / Accepted: 2 August 2017 / Published online: 5 August 2017
© Springer Science+Business Media, LLC 2017

Abstract A single phase white light emitting Dy³⁺ doped LiCaBO₃ phosphors were prepared by solid-state reaction method at 700 °C. The crystal structure properties were analyzed by utilizing powder X-ray Diffraction and followed by the profile fitting to calculate the lattice parameters. The FESEM, UV–Vis, photoluminescence excitation and emission spectra, decay time and quantum yield measurement were utilized to characterize the samples. The temperature dependent photoluminescence emission and decay times were recorded in the temperature range 100–480 K. The phosphor exhibits two emission bands at 485 nm (blue) and 578 nm (yellow) originating from the f–f transition of Dy³⁺. The optimized doping concentration for maximum emission intensity was 2 mol%. A near white emission was achieved with color co-ordinate (0.35, 0.39) and CCT value 4955 K. The material had excellent thermal and color stability. The absolute quantum yield is 0.25. So the near white emission, excellent thermal stability and suitable quantum yield of LiCaBO₃: Dy³⁺ can be a promising candidate for near UV–LED pumped white light emitting diode.

1 Introduction

After the discovery of blue LED, the research on white LED (w LED) boosted due to its high luminous efficiency, brightness, low power consumption, environmental friendliness and long stability which replaces the incandescent

lamps and fluorescent lamps [1–3]. The white light from a LED can be produced by mixing the radiation from three red, green and blue LED. Another approach is that a blue or n-UV pumped phosphor converted LED. Among them, phosphor converted LED are superior to the combination of RGB LED which required different driven voltage for various LED. Again in blue LED chip, YAG: Ce³⁺ yellow phosphor is used to convert the color from blue to white. But, YAG: Ce³⁺ have several demerits such as low color rendering index, halo effect due to lack of red component in the emission spectrum [4]. On the other way, near UV converted mixed of tri-color RGB phosphor based white LED has the disadvantage of reabsorption [5, 6]. So the single phase near UV or UV converted white LED is required in which white emission can be produced by doping a single rare earth ion (Eu²⁺, Eu³⁺ or Dy³⁺) into a suitable host to enhance the luminous efficiency of the white LED.

To meet the criteria for phosphor-converted LED, the choice of host is important. The luminescence efficiency, thermal stability, chemical stability of the phosphor depends on the physical properties of the materials [7]. LiCaBO₃ has excellent thermal stability, environmental friendliness, low-cost synthesis and strong absorption in the UV range [8]. LiCaBO₃ has an orthorhombic structure with Pbc_a space group, and Li and Ca atoms are coordinated with five or seven oxygen atoms [9].

Dy³⁺ ion has two emission bands in the visible region. One is at blue region (450–525 nm), and another one is at yellow region (525–625 nm). The blue emission is due to the ⁴F_{9/2} → ⁶H_{15/2} magnetic dipole transition, and the yellow emission is due to the ⁴F_{9/2} → ⁶H_{15/2} electric dipole transition. Among them, the ⁴F_{9/2} → ⁶H_{15/2} transition is hypersensitive (ΔL=2, ΔJ=2) which is affected by the local environment of the crystal. The ratio of yellow to blue (Y/B) depend on covalency called nephelauxetic effect

✉ Sourav Das
sourav.das1988@gmail.com

¹ Department of Applied Physics, Indian Institute of Technology (ISM), Dhanbad, Jharkhand 826004, India

between Dy^{3+} and O_2^- in the composite oxide and which is host dependent [10]. By combining the two emissions, it is possible to obtain white light in a single host material with a single activator Dy^{3+} . Consequently, the Y/B ratio in a certain host is independent of temperature. So the Dy^{3+} is a potential activator for near UV or UV converted white light-emitting diode.

In this work, LiCaBO_3 : Dy^{3+} phosphor was prepared by solid state reaction method. The structural, luminescent properties, quantum yield measurements are investigated in details. The temperature dependent photoluminescence was carried out to obtain thermal and color stability of the phosphor. So the single phase Dy^{3+} doped LiCaBO_3 can be potentially applicable to the white light emitting diode.

2 Experimental section

2.1 Preparation of $\text{LiCa}_{1-x}\text{BO}_3$: x Dy^{3+} phosphor

$\text{LiCa}_{1-x}\text{BO}_3$: x Dy^{3+} samples were prepared by high-temperature solid-state reaction method. Stoichiometric amounts of Li_2CO_3 , CaCO_3 , HBO_3 and Dy_2O_3 were mixed and grinded in a mortar pestle for 1 h with ethanol medium. Then samples were put into alumina crucibles and kept at 700 °C for 2 h at a heating and cooling rate 5 °C/min. Then, samples were grinded again in a mortar pestle to get a fine powder.

2.2 Characterization

X-ray diffraction studies were carried out on a Bruker D8 Focus diffractometer with $\text{CuK}\alpha 1$ radiation ($\lambda = 1.5406 \text{ \AA}$). The morphology of the samples was carried on a field emission microscopy (FESEM, Supra 55). Photoluminescence emission and excitation spectra had been conducted on Cary Eclipse Fluorescence Spectrophotometer (Agilent Technologies) at room temperature. Decay kinetics was measured by Cary Eclipse Fluorescence Spectrophotometer (Agilent Technologies) in the lifetime mode at room temperature. The pulsed Xenon lamp was used as the excitation source equipped with the system. The temperature dependent photoluminescence and decay kinetic were measured by attaching the Optistat DN2 Cryostat (Oxford Instruments) in the sample stage of Cary Eclipse Fluorescence Spectrophotometer. The sample used for temperature dependent measurement was in pelletized form. The temperature of the sample controlled by MercuryITC temperature controller connected to the cryostat from 100 to 480 K. Again, the absolute PL quantum yield (QY) measurement of the powder sample was conducted using PTI QM-400 fluorescence spectrophotometer system containing an integrating sphere. The powder sample was poured into the powder sample

holder grooved covered with a quartz disc, and BaSO_4 fine powder was used as reference sample. The system provided the quantum yield calculation functions that calculate the ratio of emitted to absorbed photons.

3 Results and discussion

3.1 Structural studies

Figure 1 shows the powder XRD pattern and simulated pattern of the LiCaBO_3 : 2 mol % Dy^{3+} phosphor. The material is polycrystalline nature. Debye-Scherer formula was used to calculate the crystallite size of the sample.

$$D = \frac{K\lambda}{\beta \cos \theta} = \frac{0.9\lambda}{\beta \cos \theta} \quad (1)$$

where β is the full width at half maxima, K (shape factor) = 0.9 and λ (wavelength of X-ray) = 0.154 nm.

The crystallite size was also calculated from Williamson–Hall relation given by,

$$\frac{\beta \cos \theta}{\lambda} = \frac{1}{D} + \frac{\epsilon \sin \theta}{\lambda} \quad (2)$$

where ϵ is the microstrain present in the crystal and D is the crystallite size [11, 12]. Figure 2 show the Williamson–Hall Plots.

The average crystallite size obtained from Debye–Scherer formula for the dominant peaks was 58.8 nm. The crystallite size obtained from Williamson–Hall plot was 53.76 nm. There is no standard JCPDS file found for the LiCaBO_3 compound. The XRD pattern well matched with the simulated pattern of LiCaBO_3

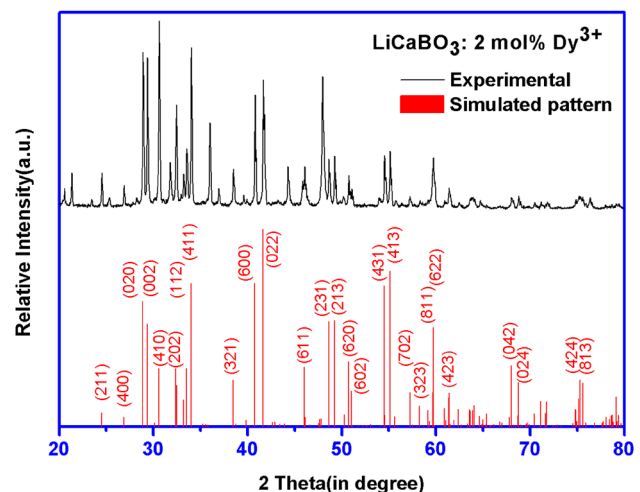


Fig. 1 Powder XRD pattern of LiCaBO_3 : 2 mol % Dy^{3+}

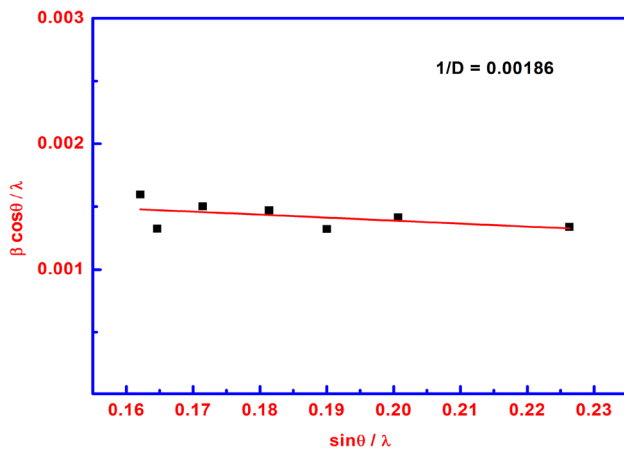


Fig. 2 The Williamson–Hall plot of $\text{LiCaBO}_3: 2 \text{ mol } \% \text{ Dy}^{3+}$

obtained by Le Bail profile fitting by Bruker TOPAS software. So the phase indexing and lattice parameters were achieved by Le Bail profile fitting program of TOPAS 4.2 Software (Bruker AXS). All of the XRD peaks of $\text{LiCaBO}_3: \text{Dy}^{3+}$ could be indexed in the orthorhombic structure with space group $Pbca$ and the lattice parameters are $a = 13.26198(39) \text{ \AA}$, $b = 6.17745(19) \text{ \AA}$, $c = 6.07834(18) \text{ \AA}$ and $V = 497.969(26) \text{ \AA}^3$. The obtained experimental powder diffraction pattern in the range of 10° – 80° are very similar with the simulated powder diffraction patterns of the previously reported LiCaBO_3 crystal structure [13, 14]. Besides the LiCaBO_3 main phase, there is some impurity phase which is due to the presence of unreacted CaCO_3 , Li_2CO_3 . The presence of impurity phase is due to relatively low-temperature anneal at 700°C of LiCaBO_3 . When the material was annealed above 700°C , the samples went to solid form either by melting Li_2CO_3 or a borate glass stage formed which kept us the annealing temperature at 700°C . Again, Dy^{3+} occupied the Ca^{2+} sites in the LiCaBO_3 host and the substitution of Ca^{2+} by Dy^{3+} did not influence the phase and crystal structure of the host.

3.2 Morphological studies

Figure 3 shows the morphology of $\text{LiCaBO}_3: \text{Dy}^{3+}$ phosphor obtained from the Field Emission Scanning Electron Microscope. The particles shapes are aggregated microspheres. The particles sizes vary from 2 to $10 \mu\text{m}$. The higher magnification image of the sample shows some flakes like structure are distributed on the surface of the microspheres.

3.3 UV–Visible diffuse reflectance study

The diffuse reflectance spectra of the undoped and dysprosium doped LiCaBO_3 samples measured in the range

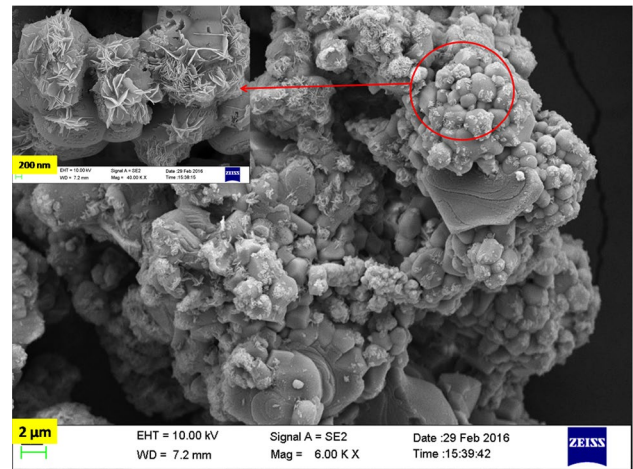


Fig. 3 FESEM image of $\text{LiCaBO}_3: \text{Dy}^{3+}$ phosphor

200 – 800 nm is presented in Fig. 4. The spectrum for undoped sample shows absorption at 220 nm corresponding to the band gap of the material. The absorption due to Dy^{3+} was not observed attributable to low doping concentration in the host matrix.

From the DR spectrum, the band gap of $\text{LiCaBO}_3: \text{Dy}^{3+}$ phosphor were determined by using the Kubelka–Munk Theory. The absorption spectrum of the phosphor was transformed to Kubelka–Munk function [15] given as:

$$F(R) = \frac{(1 - R)^2}{2R} = \frac{K}{S} \quad (3)$$

where R is the diffuse reflectance of the spectrum, K is the absorption coefficient and S is the scattering coefficient.

The well known Tauc relation relates the direct band gap (E_g) and linear absorption coefficient (α) [16]

$$\alpha h\nu = c(h\nu - E_g)^{1/2} \quad (4)$$

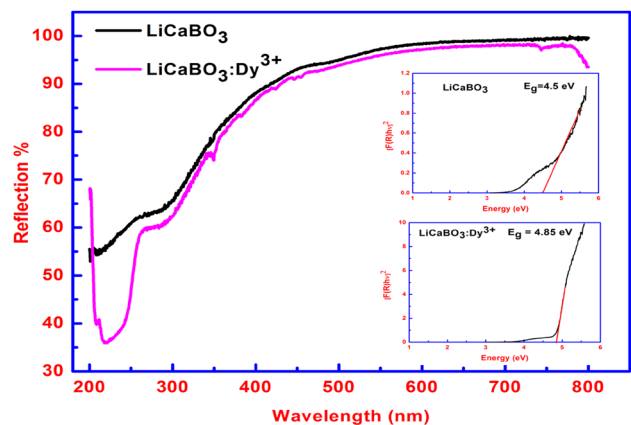


Fig. 4 UV–Vis diffuse reflectance spectra of undoped and Dy^{3+} doped LiCaBO_3 phosphor

$h\nu$ is the energy of light and C is constant. The diffuse reflectance spectrum is converted into Kubelka–Munk function by substituting $F(R_\infty)$ in place of α .

$$[h\nu F(R_\infty)]^2 = A(h\nu - E_g) \tag{5}$$

R_∞ represents the reflectance of the infinitely thick sample with respect to a reference at each wavelength, A is a constant. $h\nu$ is in eV and its relationship to the wavelength λ (in nm) becomes $h\nu = \frac{1239.7}{\lambda}$.

From the plot of $[F(R_\infty)h\nu]^2$ versus $h\nu$, the value of E_g was obtained by extrapolating the linear fitted regions to $[F(R_\infty)h\nu]^2 = 0$. The band gap calculated from the diffuse reflectance spectra using Kubelka–Munk function was found to be 4.5 eV for undoped sample and 4.85 eV for dysprosium doped sample. With Dy^{3+} doping, the band gap increases which can be explained by Burstein–Moss effect which states that as the doping concentration increases the Fermi level in the conduction band of a degenerate semiconductor shifts upwards which leads to the increase of the band gap energy [17].

3.4 Photoluminescence properties at room temperature

Figure 5 shows the excitation and emission spectra of $LiCaBO_3: 2 \text{ mol\% } Dy^{3+}$ phosphor. The excitation spectrum recorded by monitoring the emission wavelength at 578 nm. The emission spectra recorded at different excitation wavelengths. The excitation spectrum shows five peaks at 296, 324, 351, 364 and 388 nm corresponding to the intra 4f transitions from ground states $^6H_{15/2}$ to the excited states of Dy^{3+} ions, which are $^4L_{17/2}$, $^4D_{7/2}$, $^6P_{7/2}$, $^6P_{7/2}$, $^6M_{21/2}$ respectively [18]. The two emission peak at 485 and 578 nm were observed under different excitation wavelength (296, 324, 351, 364 and 388 nm). Among

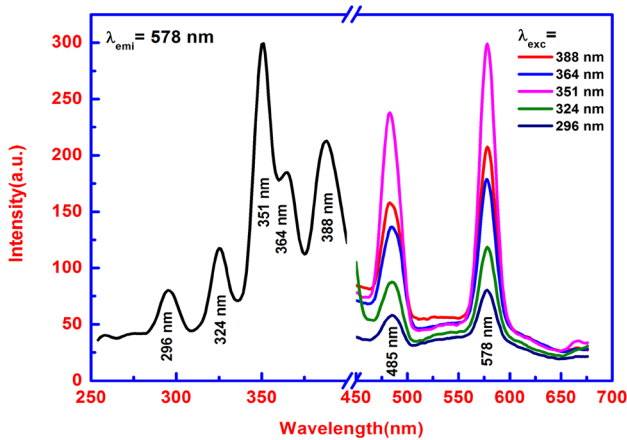


Fig. 5 The PL excitation and emission spectra of $LiCaBO_3: 2 \text{ mol\% } Dy^{3+}$ phosphor

them, dominant emission spectrum observed when excited at 351 nm. At 351 nm excitation wavelength, electrons from ground state $^6H_{15/2}$ level go to excited state $^6P_{7/2}$ level and then it quickly return to the $^4F_{9/2}$ states of Dy^{3+} ions via non-radiative transitions [19]. The blue emission at 485 nm is due to the $^4F_{9/2} \rightarrow ^6H_{15/2}$ magnetic dipole transition of Dy^{3+} ions which is less sensitive to the coordination environment of the host lattice. The comparative strong yellow band at 578 nm is due to the hypersensitive of $^4F_{9/2} \rightarrow ^6H_{13/2}$ electric dipole transition of Dy^{3+} ions [20].

The doping concentration dependent emission spectra of $LiCaBO_3: Dy^{3+}$ is shown in Fig. 6. The maximum emission intensity for both the 485 and 578 nm emission wavelength was found when the doping concentration of Dy^{3+} was 2 mol%. After a certain concentration, the concentration quenching occurred. The concentration quenching occurred due to the energy transfer between the activator ions of Dy^{3+} ascribed to the cross-relaxation mechanism [20, 21].

As the yellow band at 578 nm is due to the $^4F_{9/2} \rightarrow ^6H_{13/2}$ hypersensitive transition of Dy^{3+} , its intensity depends on the surrounding local structural environment. To investigate the asymmetry of the two peaks (blue and yellow), the asymmetry ratio was calculated by the following equation:

$$A_{21} = \frac{Y}{B} = \frac{\int_{550}^{610} I_2(\lambda) d\lambda}{\int_{460}^{505} I_1(\lambda) d\lambda} \tag{6}$$

where I_1 and I_2 are intensities for the following $^4F_{9/2} \rightarrow ^6H_{15/2}$ (B) and $^4F_{9/2} \rightarrow ^6H_{13/2}$ (Y) transitions of Dy^{3+} .

The Y/B ratio for different doping concentration of Dy^{3+} (1–4 mol%) are 0.73, 1.34, 1.28 and 1.11 respectively. According to Q. Su et al. the Y/B ratio of Dy^{3+} does vary when the Dy^{3+} is substituted for an element with different valency [22]. In our case Dy^{3+} ion is substituted with the

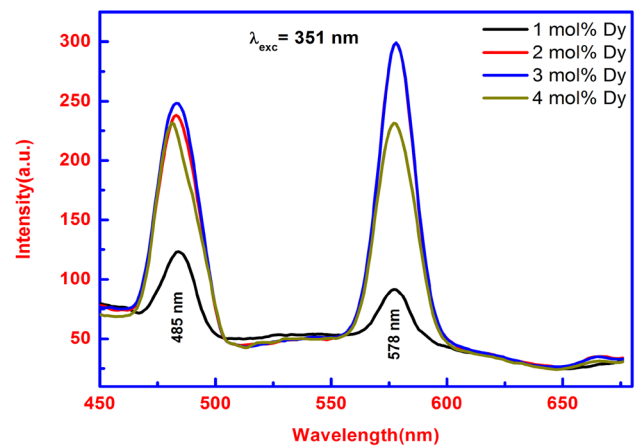


Fig. 6 The PL emission spectra of $LiCaBO_3: Dy^{3+}$ phosphor with different doping concentration of Dy^{3+}

Ca^{2+} ion in LiCaBO_3 : Dy^{3+} host matrix. So defects formed due to the surrounding and local symmetry of Dy^{3+} are changes with increasing Dy^{3+} concentrations.

Figure 7 shows the decay curve of Dy^{3+} doped LiCaBO_3 phosphor excited at 351 nm with emission wavelength monitored at 485 nm and 578 nm respectively. The resultant decay curves were fitted bi-exponential decay function:

$$I(t) = A_1 e^{-\frac{t}{\tau_1}} + A_2 e^{-\frac{t}{\tau_2}} + I_0 \quad (7)$$

where $I(t)$ is the luminescence intensity at time t , A_1 and A_2 are constants, τ_1 and τ_2 are decay constants for the exponential components, respectively. The effective lifetime can be evaluated from the equation:

$$\tau_{\text{eff}} = \frac{A_1 \tau_1^2 + A_2 \tau_2^2}{A_1 \tau_1 + A_2 \tau_2} \quad (8)$$

The bi-exponential decay occurred in the studied samples due to the nonuniform distribution of Dy^{3+} ions in the host matrix. The effective lifetime calculated for the 1–4 mol% Dy^{3+} doped LiCaBO_3 for 485 nm emission are 0.883, 0.683, 0.673 and 0.592 ms. The effective lifetime for 578 nm emission are 0.896, 0.674, 0.661 and 0.584 ms respectively. The decrease in an effective lifetime with the increase of Dy^{3+} concentrations may be due to the exchange interaction among the excited Dy^{3+} – Dy^{3+} ions. The lifetime parameters at the emission wavelength of 485 and 578 nm for different concentrations are shown in Table 1.

Table 1 Decay parameters at room temperature with different concentrations of Dy^{3+}

Dy^{3+} doping concentration	τ_1 (ms)	485 nm τ_2 (ms)	τ_1 (ms)	578 nm τ_2 (ms)
1 mol%	0.884	0.884	0.360	0.945
2 mol%	0.266	0.792	0.269	0.780
3 mol%	0.341	0.832	0.323	0.799
4 mol%	0.298	0.672	0.265	0.650

Figure 8 shows the CIE diagram of LiCaBO_3 : Dy^{3+} phosphor at different Dy^{3+} concentrations. To calculate the color parameters, the Commission International de l'Eclairage (CIE) color co-ordinates and Color Correlated Temperature (CCT) were calculated using the standard formula with the help of color calculator software.

The chromaticity co-ordinates can be calculated by the following tri-stimulus values. In the case of CIE 1931-XYZ tri chromatic system the tri-stimulus values are defined as [23]

$$X = \int_{380 \text{ nm}}^{780 \text{ nm}} I(\lambda) \bar{x}(\lambda) d\lambda \quad (9)$$

$$Y = \int_{380 \text{ nm}}^{780 \text{ nm}} I(\lambda) \bar{y}(\lambda) d\lambda \quad (10)$$

$$Z = \int_{380 \text{ nm}}^{780 \text{ nm}} I(\lambda) \bar{z}(\lambda) d\lambda \quad (11)$$

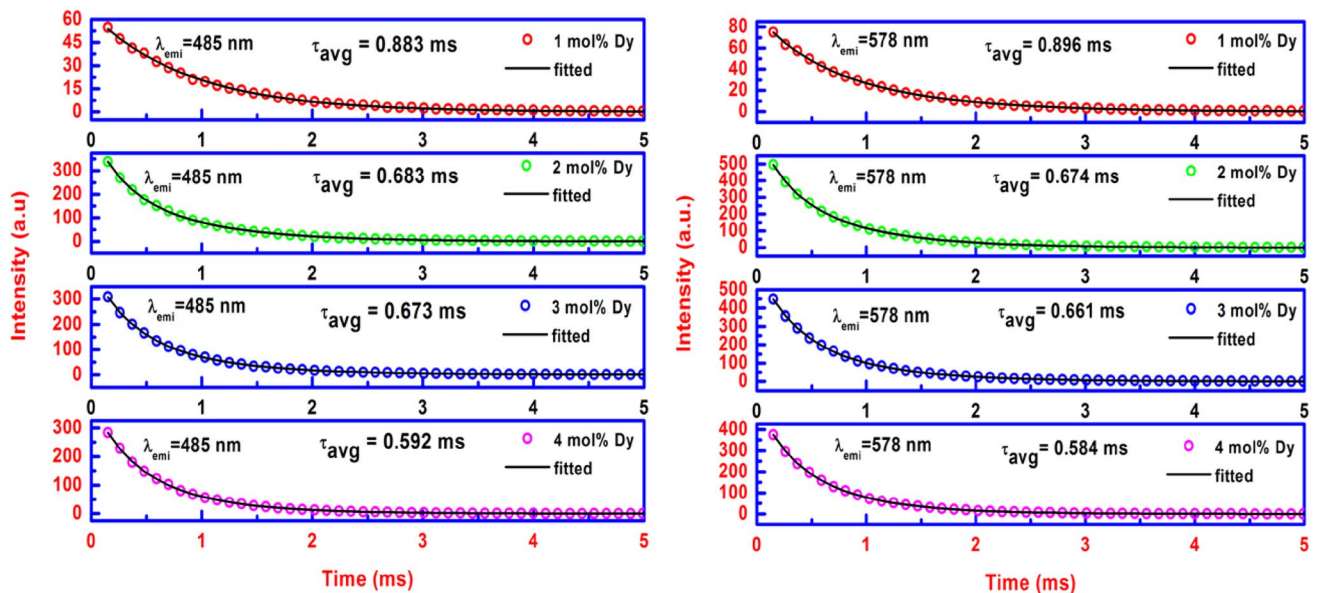


Fig. 7 Decay curve of LiCaBO_3 : Dy^{3+} phosphor with different doping concentration of Dy^{3+} monitored at 485 and 578 nm emission wavelengths

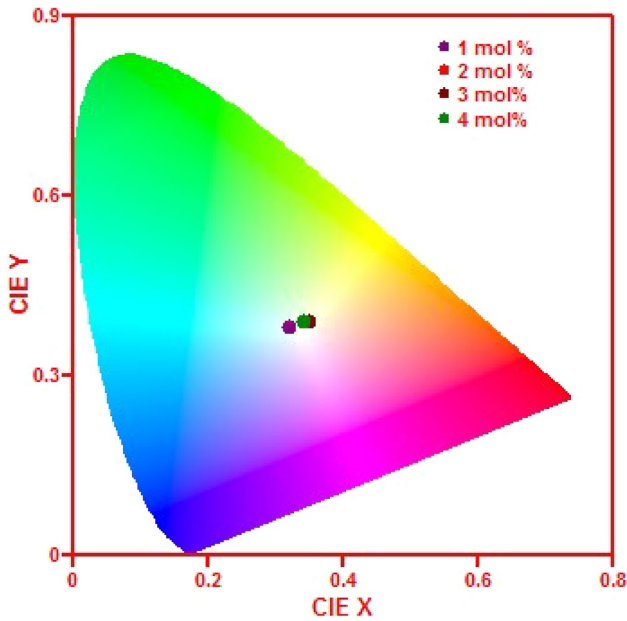


Fig. 8 The CIE diagram of LiCaBO₃: Dy³⁺ phosphor with different doping concentration of Dy³⁺

where $I(\lambda)$ is the spectral intensity of the material, while $\bar{x}(\lambda)$, $\bar{y}(\lambda)$, $\bar{z}(\lambda)$, are the chromatic functions of the observer defined by CIE.

The chromaticity co-ordinates are defined as [24]

$$x = \frac{X}{X+Y+Z} \tag{12}$$

$$y = \frac{Y}{X+Y+Z} \tag{13}$$

$$z = \frac{Z}{X+Y+Z} \tag{14}$$

where $x + y + z = 1$, thus it is enough to describe the chromaticity with two numbers usually x and y .

The quality of white light in terms of color correlated temperature (CCT) is given by the McCamy empirical formula [25]

$$CCT = -437n^3 + 3601n^2 - 6861n + 5514.31 \tag{15}$$

Table 2 The CIE co-ordinates and CCT values of LiCaBO₃: Dy³⁺ phosphor with different doping concentration of Dy³⁺

Dy ³⁺ doping concentration	Color co-ordinates (x, y)	CCT (K)
1 mol%	(0.32, 0.38)	5955
2 mol%	(0.35, 0.39)	4955
3 mol%	(0.35, 0.39)	4955
4 mol%	(0.34, 0.39)	5267

where $n = (x - x_e)/(y - y_e)$ is the inverse slope line and chromaticity epicenter is at $x_e = 0.3320$ and $y_e = 0.1858$.

The color co-ordinates value (x, y) lies in the near white region and varies slightly with Dy³⁺ doping concentration. The CCT values vary from 4955 to 5955 K which will be suitable for near UV converted white light-emitting diode. The CIE co-ordinates and CCT values are listed in Table 2.

The absolute fluorescence quantum yield, η , is, by definition, the ratio of the number of photons emitted to the number of photons absorbed [26]:

$$\eta = \frac{N^{em}}{N^{abs}} \tag{16}$$

so, from Eq. (16), the luminescence quantum yield can be expressed by ratio of difference in area under the curve of emission intensity of sample and reference to the difference in area of scattered intensity curve of reference and sample, at excitation wavelength.

The absolute fluorescence quantum yield can be expressed by the following equation:

$$\eta = \frac{E_B - E_A}{S_A - S_B} \tag{17}$$

where E_B is integral emission intensity of the sample, E_A is the integral emission intensity of the reference, S_A is the integral scattered intensity of the reference and S_B is the integral scattered intensity of sample. Here, BaSO₄ powder was used as reference.

Figure 9 shows the quantum yield measurement for the LiCaBO₃: 2 mol% Dy³⁺ phosphor sample. The sample was excited at 350 nm. In Fig. 9, S_A is scattered intensity of reference at 350 nm and S_B is scattered intensity of sample at 350 nm. From difference of area under the curve, we have

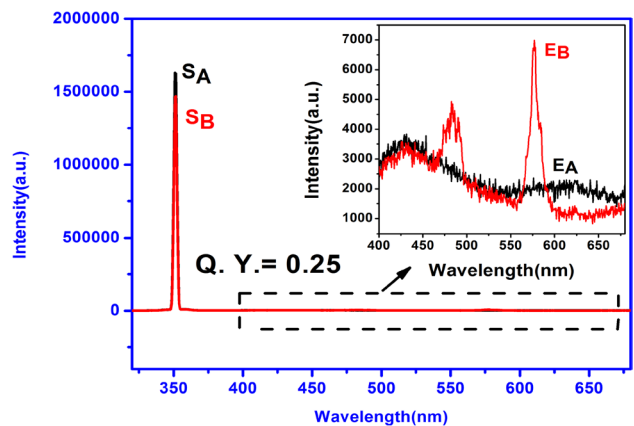


Fig. 9 Scattered emission intensity of the reference sample (black) and scattered emission intensity of the sample (red) for quantum yield measurement. (Color figure online)

calculated the absorbption of the sample. E_B is the emission curve of the sample and E_A is the emission curve of the reference when excited at 350 nm (shown in inset of Fig. 9). From difference of area under emission curve of sample and reference, the net emission of the sample have been calculated. The resulting ratio of emission to absorbption gives the calculated quantum yield (η) is 0.25.

3.5 Temperature dependent photoluminescence properties

Figure 10a shows the emission spectra of $\text{LiCaBO}_3: 2 \text{ mol\% Dy}^{3+}$ phosphor excited at 351 nm recorded at a temperature range from 100 K to 480 K. The emission consists of two peaks. The peak centered at 483 nm is due to the ${}^4\text{F}_{9/2} \rightarrow {}^6\text{H}_{15/2}$ magnetic dipole transition, and the peak centered at 578 nm is due to the ${}^4\text{F}_{9/2} \rightarrow {}^6\text{H}_{13/2}$ electric dipole transition which is hyper sensitive to the local environments. Figure 10b, c shows the variation of integrated intensity and FWHM of the peak centered at 578 nm with temperature

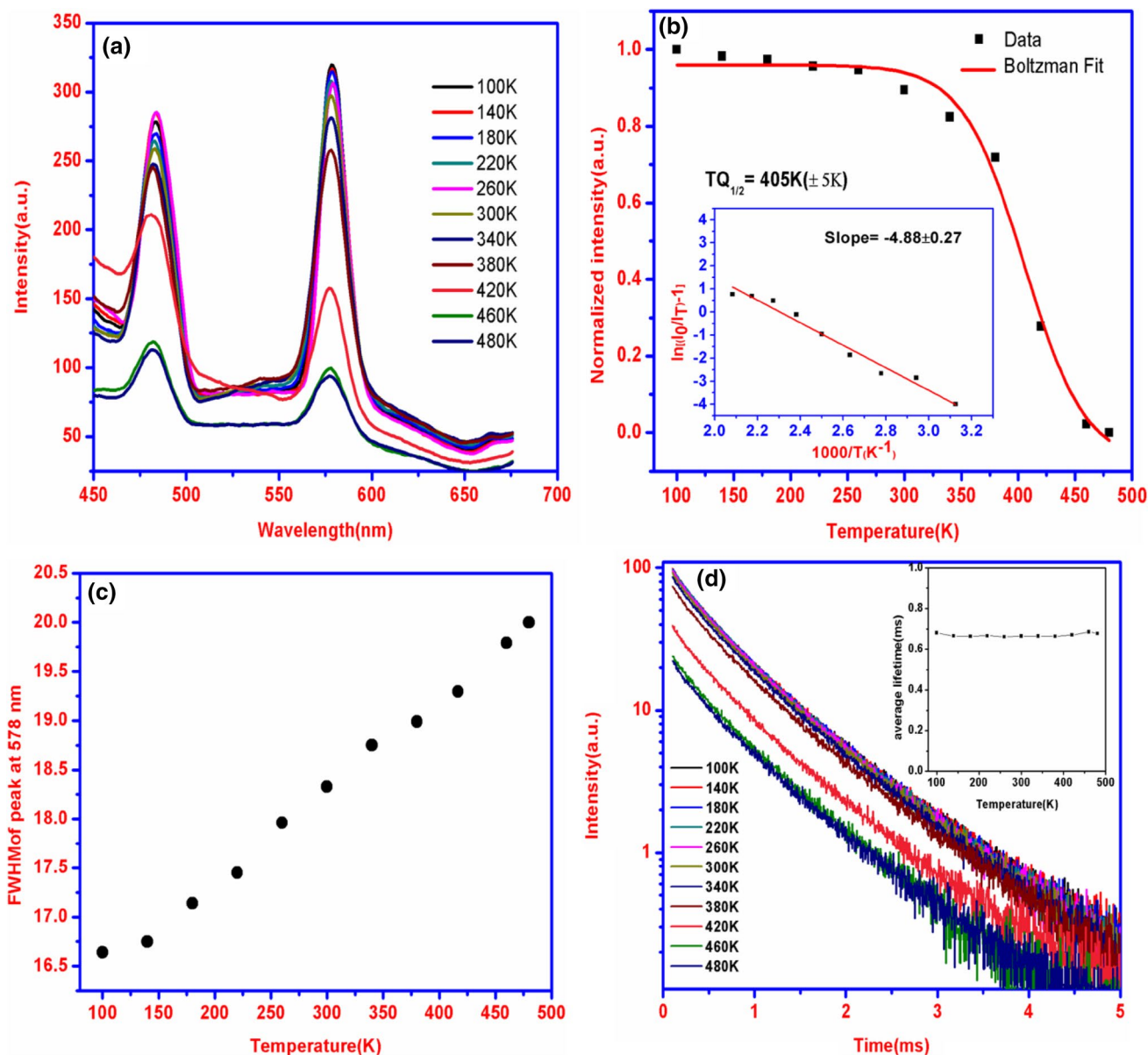


Fig. 10 a Temperature dependent photoluminescence emission spectra ($\lambda_{\text{exc}} = 351 \text{ nm}$), b calculation of $TQ_{1/2}$ value, c variation of FWHM with temperature for the peak 578 nm and d temperature dependent photoluminescence decay of $\text{LiCaBO}_3: 2 \text{ mol\% Dy}^{3+}$ phosphor

respectively. The integral emission intensity (at 578 nm) is decreased with increasing temperature from which the thermal stability of the phosphor can be explained. The thermal stability of a phosphor is defined by thermal quenching temperature $T_{Q_{1/2}}$, i.e. the temperature at which the PL emission intensity is half of its initial intensity [27, 28]. The thermal quenching temperature $T_{Q_{1/2}}$ was obtained by Boltzmann sigmoidal fit [29]:

$$y(T) = A_2 + \frac{A_1 - A_2}{1 + e^{(T-T_{1/2})/dT}} \quad (18)$$

where $y(T)$ is the normalized emission intensity at a given temperature T (in K), A_1 and A_2 is the initial and final emission intensity value, here we normalized the emission intensity value between 1 and 0, so the $A_1 = 1$, $A_2 = 0$. $T_{1/2}$ is the centre of the sigmoid; dT is the changes in T [30]. The fitted curve is shown in Fig. 6b. The calculated $T_{Q_{1/2}}$ value from the fitted result is 405 K which is higher than the 393 K, the required temperature stability for high power LED. The activation energy was calculated from the temperature dependent emission spectrum according to the following equation [31]:

$$I_T = \frac{I_0}{[1 + c \exp(-\Delta E/kT)]} \quad (19)$$

where I_0 is the intensity at 300 K and I_T is the intensity at temperature T , c is a constant, k is the Boltzmann constant (8.67×10^{-5} eV K^{-1}) and ΔE is the activation energy. The results of linear fitting of $\ln[(I_0/I_T) - 1]$ versus $1000/T$ gives the value of slope from which the calculated activation energy is 0.42 eV (shown in inset of Fig. 10b).

The broadening of the peak is evaluated by calculating the FWHM of the peak. The value of the FWHM is increasing with rising temperature from 100 to 480 K for the peak centered at 578 nm (shown in Fig. 10c). The width of the emission band and thermal quenching is related to the configuration co-ordination model. The FWHM increase and emission intensity decrease with increasing temperature for the ${}^4F_{9/2} \rightarrow {}^6H_{13/2}$ transition is due to the non-radiative transition. The non radiative transition probability increases with increasing temperature resulting in the decrease of emission intensity due to crossover process [31]. Consequently, the FWHM broadening of emission is due to dominating nature of electron–phonon interaction at high temperature.

Figure 10d shows the influence of temperature on the decay time. The decay curves were fitted bi-exponentially according to Eq. (7). The average lifetime were calculated according to Eq. (8). The average lifetimes are almost constant and not influenced by the temperature. The average lifetime is 0.67 ms. The disaffect of temperature on the lifetime agreed with the previously report [32].

4 Conclusion

A white light emitting Dy^{3+} doped $LiCaBO_3$ phosphor was prepared by solid state reaction method. The Le-Bail profile fitting ascribed that $LiCaBO_3$ has an orthorhombic structure with $Pbca$ space group. The Dy^{3+} occupied the Ca^{2+} sites in the $LiCaBO_3$ host. From the microstructure analysis, the particles shapes are aggregated microsphere with particle sizes 2–10 μm . The band gap of the phosphor is 4.85 eV. The photoluminescence emission spectrum shows two emission peaks at 485 and 578 nm, which are due to the ${}^4F_{9/2} \rightarrow {}^6H_{15/2}$ magnetic dipole transition and ${}^4F_{9/2} \rightarrow {}^6H_{13/2}$ hypersensitive electric dipole transition. The maximum PL emission intensity was observed for 3 mol% Dy^{3+} doping. The yellow to blue emission ratio varies with concentration due to valency difference between Dy^{3+} ions which substitute the Ca^{2+} ions in the host. The dependence of lifetime with Dy^{3+} concentrations may be due to exchange interaction among the excited Dy^{3+} – Dy^{3+} ions. The temperature dependent photoluminescence shows that the materials have excellent thermal stability. The color of the phosphor lies in the near white region, and CCT values vary from 4955 to 5955 K. The thermal quenching temperature is 405 K. The quantum yield of the phosphor is 0.25. The above results indicate that the Dy^{3+} doped $LiCaBO_3$ can be a potential phosphor for single phase host near UV converted white light emitting diode.

Acknowledgements The authors acknowledge DST-FIST facility (Project No. SR/FST/PSI-004/2013) for using lifetime spectrophotometer.

References

1. S. Nakamura, T. Mukai, M. Senoh, Candela-class high brightness InGaN/AlGaIn diode-heterostructures blue-light-emitting diodes. *Appl. Phys. Lett.* **64**, 1687 (1994)
2. Z. Xia, Z. Xu, M. Chen, Q. Liu, Recent developments in the new inorganic solid state LED phosphors. *Dalton Trans.* **45**, 11214–11232 (2016)
3. J. Li, J. Yan, D. Wen, W.U. Khan, J. Shi, M. Wu, Q. Su, P.A. Tonner, Advanced red phosphors for white light-emitting diodes. *J. Mater. Chem. C* **4**, 8611–8623 (2016)
4. F. Liu, Q. Liu, Y. Fang, N. Zhang, B. Yang, G. Zhao, White light emission from $NaLa(PO_3)_4: Dy^{3+}$ single-phase phosphors for light emitting diodes. *Ceram. Int.* **41**, 1917–1920 (2015)
5. H. Liu, L. Liao, M.S. Molohev, Q. Guo, Y. Zhang, L. Mei, A novel single-phase white light emitting phosphors $Ca_9La(PO_4)_5(SiO_4)F_2: Dy^{3+}$: synthesis, crystal structure and luminescence properties. *RSC Adv.* **6**, 24577–24583 (2016)
6. C. Zhao, D.C. Zhu, M.J. Tu, M. Huang, L.L. Peng, T. Han, A novel near-ultraviolet (NUV) converting blue-violet $Ca_{2-x}AlMg_{0.5}Si_{1.5}O_7: x Ce^{3+}$ phosphor for white light emitting diodes (w-LEDs). *RSC Adv.* **6**, 2368–2373 (2016)

- R.J. Xie, N. Hirosaki, K. Sakuma, N. Kimura, White light-emitting diodes (LEDs) using (oxy) nitride phosphors. *J. Phys. D* **41**, 144013 (2008)
- C. Guo, J. Yu, X. Ding, M. Lai, Z. Ren, J. Bai, A dual-emission phosphor LiCaBO_3 : Ce^{3+} , Mn^{2+} with energy transfer for near-UV LEDs. *J. Electrochem. Soc.* **158**, J42–J46 (2011)
- S. Tamboli, B. Rajeswari, S.J. Dhoble, Investigation of UV-emitting Gd^{3+} -doped LiCaBO_3 phosphor. *Luminescence* **31**, 551–556 (2016)
- M. Shang, C. Li, J. Lin, How to produce white light in a single phase host? *Chem. Soc. Rev.* **43**, 1372–1386 (2014)
- S.B. Oadri, J.P. Yang, E.F. Skelton, B.R. Ratna, Evidence of strain and lattice distortions in lead sulfide nanocrystallites. *Appl. Phys. Lett.* **70**, 1020 (1997)
- G.K. Williams, W.H. Hall, X-ray line broadening from filed aluminum and wolfram. *Acta. Metal.* **1**, 2–31 (1953)
- L. Wu, X.L. Chen, H. Li, M. He, L. Dai, X.Z. Li, Y.P. Xu, Structure determination of a new compound LiCaBO_3 . *J. Solid State Chem.* **177**, 1111–1116 (2004)
- W. Zhou, D. Hou, F. Pan, B. Zhang, P. Dorenbos, Y. Huang, Y. Tao, H. Liang, VUV-vis photoluminescence, X-ray radioluminescence and energy transfer dynamics of Ce^{3+} and Pr^{3+} doped LiCaBO_3 . *J. Mater. Chem. C* **3**, 9161–9169 (2015)
- A. Mondal, S. Das, J. Manam, Hydrothermal synthesis, structural and luminescent properties of a Cr^{3+} doped MgGa_2O_4 near infrared long lasting nanophosphors. *RSC Adv.* **6**, 82484–82495 (2016)
- J. Tauc, A. Mentsh, States in the gap. *J. Non-Cryst. Solids* **8**, 569–585 (1972)
- M. Chowdhury, S.K. Sharma, Spectroscopic behaviour of Eu^{3+} in SnO_2 for solid state lighting devices. *RSC Adv.* **5**, 51102–51109 (2015)
- P. Li, Z. Wang, Z. Yang, Q. Guo, X. Li, Luminescent characteristics of LiCaBO_3 : $\text{M}(\text{M} = \text{Eu}^{3+}, \text{Sm}^{3+}, \text{Tb}^{3+}, \text{Ce}^{3+}, \text{Dy}^{3+})$ for white LED. *J. Lumin.* **130**, 222–225 (2010)
- P. Kumari, J. Manam, Structural, optical and special spectral changes of Dy^{3+} in orthovanadates. *RSC Adv.* **5**, 107575–107584 (2015)
- A.K. Bedyal, V. Kumar, R. Prakash, O.M. Ntwaeaborwa, H.C. Swart, A near-UV converted LiMgBO_3 : Dy^{3+} nanophosphors: surface and spectral investigations. *Appl. Surf. Sci.* **329**, 40–46 (2015)
- G. Blasse, B.C. Grabmaier, *Luminescent Materials*. (Springer, New York, 1994)
- Q. Su, Z. Pei, L. Chi, H. Zhang, Z. Zhang, F. Zou, The yellow-to-blue intensity ratio of Dy^{3+} emission. *J. Alloys Compd.* **192**, 25–27 (1993)
- T. Smith, J. Guild, The CIE colorimetric standards and their use. *Trans. Opt. Soc.* **33**, 73 (1931)
- J. Schanda, *Colorimetry: Understanding the CIE System*. (Wiley, New York, 2007)
- S. Dutta, S. Som, S.K. Sharma, Luminescence and photometric characterization of K^+ compensated CaMoO_4 : Dy^{3+} nanophosphors. *Dalton Trans.* **43**, 9654–9661 (2013)
- N. S. Singh, R. S. Ningthoujam, N. Yaiphaba, S. D. Singh, R. K. Vasta, Luminescence, lifetime and quantum yield studies of redispersible Eu^{3+} -doped GdPO_4 crystalline nanoneedles: Core-shell and concentrations effects. *J. App. Phys.* **105**, 064303 (2009).
- J. Sun, D. Cui, Synthesis, structure and thermally stable luminescence of Dy^{3+} -doped $\text{Na}_3\text{YSi}_2\text{O}_7$ host compound. *J. Am. Ceram. Soc.* **97**, 843–847 (2014)
- Y.Y. Ma, F. Xiao, S. Xe, Q.Y. Zhang, Z.H. Jiang, The effect of zinc acetate dehydrate on morphology and luminescence properties of $\text{CaSi}_2\text{O}_2\text{N}_2$: Eu^{2+} phosphor. *J. Am. Ceram. Soc.* **96**, 2238–2244 (2013)
- J. Aguiar, P. Carpena, J.A. Molina-Bolivar, C. Carnero Ruiz, On the determination of critical concentration by the pyrene 1: 3 ratio method. *J. Colloid Interface Sci.* **258**, 116–122 (2003)
- M. Janulevicius, P. Marmokas, M. Misevicius, J. Grigorjevaite, L. Mikoliunaite, S. Sakirzanovas, A. Katelnikovas, Luminescence and luminescence quenching of highly efficient $\text{Y}_2\text{Mo}_4\text{O}_{15}$: Eu^{3+} phosphors and ceramics. *Sci. Rep.* **6**, 26098 (2016)
- W.H. Fonger, C.W. Struck, Eu^{3+} ^5D resonance quenching to the charge-transfer states in $\text{Y}_2\text{O}_2\text{S}$, $\text{La}_2\text{O}_2\text{S}$ and LaOCl . *J. Chem. Phys.* **52**, 6364 (1970)
- C. Liu, Z. Qi, C.-G. Ma, P. Dorenbos, D. Hou, S. Zhang, X. Kuang, J. Zhang, H. Liang, High light yield of $\text{Sr}_8(\text{Si}_4\text{O}_{12})\text{Cl}_8$: Eu^{2+} under X-ray excitations and its temperature dependent luminescence characteristics. *Chem. Mater.* **26**, 3709–3715 (2014)